TOPICAL REVIEW — 2D materials: physics and device applications

Toward high-performance two-dimensional black phosphorus electronic and optoelectronic devices*

Xuefei Li(李学飞)[1], Xiong Xiong(熊雄)[2], and Yanqing Wu(吴燕庆)[1,2,†]

[1] Wuhan National High Magnetic Field Center and School of Electrical and Electronic Engineering, Huazhong University of Science and Technology, Wuhan 430074, China

[2] Wuhan National High Magnetic Field Center and School of Optical and Electronic Information, Huazhong University of Science and Technology, Wuhan 430074, China

(Received 5 January 2017; revised manuscript received 13 February 2017; published online 24 February 2017)

Recently, black phosphorus (BP) has joined the two-dimensional material family as a promising candidate for electronic and photonic applications due to its moderate bandgap, high carrier mobility, and unusual in-plane anisotropy. Here, we review recent progress in BP-based devices, such as field-effect transistors, contact resistance, quantum transport, stability, photodetector, heterostructure, and in-plane anisotropy. We also give our perspectives on future BP research directions.

Keywords: black phosphorus, transistors, mobility, photodetector

PACS: 73.63.–b, 85.30.–z **DOI:** 10.1088/1674-1056/26/3/037307

1. Introduction

The experimental demonstration of graphene has opened up a window to the two-dimensional (2D) world of materials.[1] This has subsequently triggered a surge of research interest on various 2D crystals including hexagonal-boron nitride (h-BN),[2,3] transition metal dichalcogenides (TMDs, such as MoS_2 and WSe_2),[4] and black phosphorus (BP),[5,6] covering the category from insulator to narrow bandgap semiconductor. The ease of preparing these 2D crystals using mechanical exfoliation for demonstrating various prototype applications relies on the layered structures where adjacent layers are held together by the relatively weak van der Waals bonds.[7,8]

An inherent advantage of 2D materials for electronic applications is greatly improved short channel effect at the scaling limit due to their atomically thin channel.[9,10] Despite the excellent mobility of graphene, its gapless nature makes it unsuitable for logic switching, which severely limits its potential for electronic circuits. In 2011,[11] layered TMDs with tunable bandgap properties provided a new option to build ultimately scaled channel device.[4,12] Much progress has been achieved in TMDs-based FETs,[13–15] logical devices,[16,17] and optoelectronic structures.[18,19] However, the majority of the reported TMDs transistors, such as MoS_2, have a low carrier mobility and the performance of these devices is inferior to traditional semiconductors such as silicon or GaAs.[20–22] The quest for a new material that bridges the gap between graphene and TMDs is highly desired. Layered BP is an emerging 2D semiconductor with a decent bandgap and high carrier mobility.[5,6,23] Meanwhile, BP exhibits widely tunable and direct bandgap from 0.3 to 2 eV and remarkable in-plane anisotropic electrical and optical properties.[24–26] Therefore, 2D layered BP has attracted significant amount of research interest as a promising candidate for high-performance deeply-scaled electronics and optoelectronic devices.

In this review, we first discuss some of the most important characteristics of BP transistors including contact resistance, high-frequency operations, quantum transport, and stability. We also present the recent progress in electronics and optoelectronics application, including photodetectors, van der Waals heterojunction devices, and anisotropic properties. Lastly, we provide our perspective on the opportunities and challenges in this research area.

2. Basic structure properties

BP is a single-elemental layered material, which has three crystalline structures: orthorhombic, simple cubic, and rhombohedral.[27,28] The research on bulk BP could be tracked back to a century ago and the progress remained slow for many years.[23,29] Following the successful exfoliation of few-layer BP in 2014,[5] a surge of research interest has been focused on this nanomaterial and excellent electrical properties have been demonstrated. Theory predicts that the room temperature intrinsic hole mobility can be up to 10^4 $cm^2/(V{\cdot}s)$. The atomistic models of few-layer BP are presented in Fig. 1(a).[27] For each single layer, each phosphorus atom is covalently bonded with three adjacent phosphorus atoms to form a puckered honeycomb structure and the thickness of monolayer BP (named phosphorene) is ~ 5 Å. The x and y directions in the BP structure correspond to the armchair and zigzag directions of BP, respectively. It is of interest that the different effective mass

*Project supported by the National Natural Science Foundation of China (Grant Nos. 11404118, 61574066, and 61390504).

†Corresponding author. E-mail: yqwu@hust.edu.cn

© 2017 Chinese Physical Society and IOP Publishing Ltd

along different directions results in in-plane anisotropic electrical and optical properties, which is very unique in 2D materials family.[6,30–32] Figure 1(b) shows the band structure calculations for BP with various thickness.[27,33] Compared to graphene and TMDs, the bandgap of BP is strongly dependent on thickness due to quantum confinement, ranging from ~ 0.3 eV for the bulk to ~ 2.0 eV for the monolayer.[25,34,35] This wide tunable bandgap provides an advantage to optimize the performance of BP-based nanoelectronics and optoelectronics by thickness.

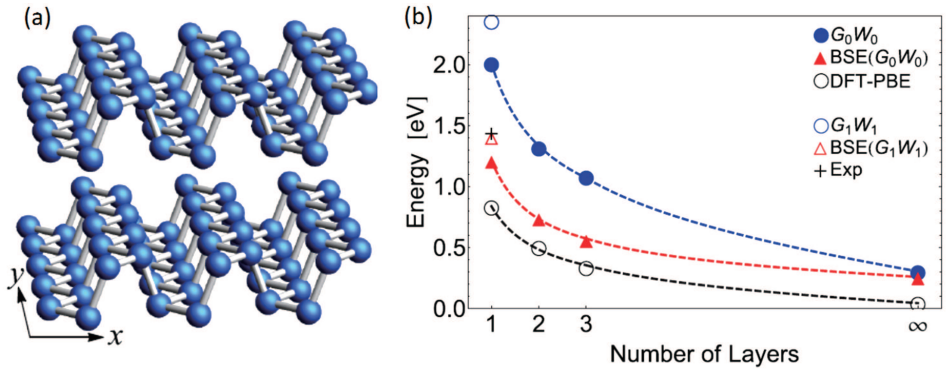


Fig. 1. (color online) (a) The ball-stick model of few-layer BP. The x, y direction is in-plane vibration along the armchair and zigzag direction, respectively. (b) Band gap of different layer numbers of few-layer BP calculated by different methods. The dashed lines are power-law fitting curves.[27]

3. Electronics properties

BP is a p-type 2D semiconductor, which has high hole mobility up to 1000 $cm^2/(V{\cdot}s)$ at room temperature, as demonstrated experimentally. Although much progress has been achieved, many challenges still exist toward electronic and optoelectronic applications. In this section, we review the electrical transport properties, contact resistance, channel length scaling, and high-frequency performance. The novel quantum transport and the development of BP passivation are also discussed.

3.1. Field-effect transistors

The first few-layer BP field-effect transistor (FET) was reported by Li *et al*, exhibiting on/off ratio of 10^5 and mobility up to 1000 $cm^2/(V{\cdot}s)$ at room temperature.[5] Figure 2(a) shows a schematic view of BP back-gated devices with 90 nm SiO_2 as gate dielectric. The field-effect mobility and Hall mobility of BP at different temperatures are shown in Fig. 2(b). The mobility of an 8-nm-thick sample first increases with decreasing temperature due to reduced electron–phonon scattering, then saturates around 300–400 $cm^2/(V{\cdot}s)$ when temperature is below 100 K due to the dominated charge impurities scattering. Liu *et al.* also reported the similar results on BP transistors shortly after the first BP publication.[6] Figure 2(c) presents the transfer characteristics of BP transistor with a channel thickness of ~ 5 nm. A current on/off ratio of ~ 10^4 and a hole mobility of 286 $cm^2/(V{\cdot}s)$ at room temperature can be achieved. As expected, the field-effect mobility shows a strong thickness dependence, as shown in Fig. 2(d), which can be explained by screening and interlayer coupling in layered materials, as proposed in several previous studies. Also, a complementary metal oxide semiconductor (CMOS) inverter with combination of BP pMOS transistors and MoS_2 nMOS transistors was demonstrated, showing great potential for BP in future electronic, optoelectronic, and flexible electronic devices. The anisotropic electronic transport is a unique property for few-layer BP,[36] which was demonstrated both theoretically and experimentally. The theory calculations show that the effective mass of electrons and the hole is $m_e \approx m_h \approx 0.3m_0$ along the armchair direction and $m_e \approx 2.6m_0$, $m_h \approx 8.3m_0$ along the zigzag direction.[6,37] This anisotropic property is further supported by polarization-resolved Raman scattering.[38] Raman results show that the measurable peak positions are independent of polarization, while the relatively intensity of the A_g^1 and A_g^2 modes varies significantly with polarization directions. This provides a useful method to determine the crystalline direction of few-layer BP flakes. The DC conductivity and IR relative extinction measured along six directions on the BP flake as shown in Fig. 2(e) show a ratio of 1.5 for the maximum value at the x-direction at the band edge and minimum value at the y-direction at the band edge.[38] This is consistent with a Hall mobility of 650 and 400 $cm^2/(V{\cdot}s)$ for holes along the light (x) and heavy (y) effective mass directions at 300 K for 15-nm-thick BP (Fig. 2(f)). Theoretical investigations show that BP transistors can meet the International Technology Roadmap for Semiconductor (ITRS) target at the 5-nm technology node.[39] The performance of BP transistors has been improved with the device optimization. The maximum extrinsic transconductance (g_m) is over 250 μS/μm for locally back-gated BP p-type transistors with 7-nm-thick HfO_2 as gate dielectrics.[40] Subthreshold slope value as low as 126 mV/decade was also achieved for a 4-nm-thick back-gated sample.[41] Du *et al.* used a chemical doping to reduce the resistance and improve the on-state current from 211 to 532 μA/μm.[42] Recently, Li *et al.* demon-

strated a high current density of 580 μA/μm for 10-nm-thick BP transistors with scandium contacts after 400 K vacuum annealing.[43] Besides the traditional oxide substrate, the flexible BP amplitude-modulated demodulator was reported by Zhu *et al.* which can endure 5000 bending cycles with minimal performance degradations.[44]

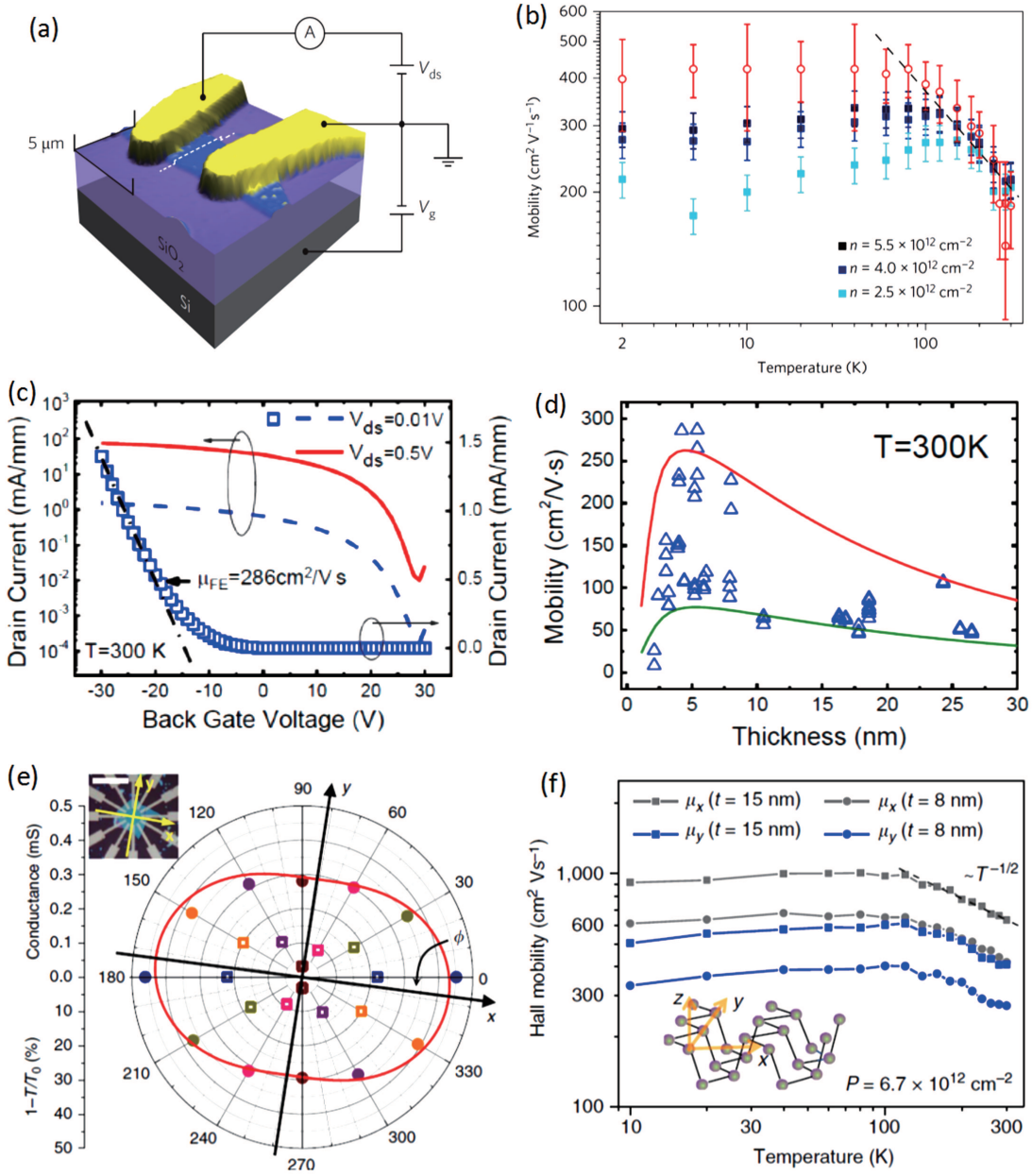


Fig. 2. (color online) (a) Schematic of device structure of a few-layer BP back gate FET.[5] (b) Field-effect mobility (red open circles with error bar) and Hall mobility (filled squares with error bar, three different values of n) as a function of temperature on a logarithmic scale. A power-law dependence $\mu \approx T^{-0.5}$ (black dashed line) is plotted in the high-temperature region as a guide to the eye.[5] (c) Transfer curves of a typical few-layer BP transistor with a film thickness of ~ 5 nm.[6] (d) Mobility summary of few-layer BP transistors with varying thicknesses.[6] (e) DC conductivity and IR relative extinction measured along the same six directions on a BP flake in polar coordinates. The optical image of this device was in the inset figure.[24] (f) Hall mobility measured at a constant hole doping concentration of 6.7×10^{12} cm^{-2} along the x and y directions for BP thin films with a thickness of 8 and 15 nm, respectively.[24]

Although most of the studies focus on p-type BP devices due to its high hole mobility, some work demonstrated that BP thin film could exhibit ambipolar or n-type transport properties. Liu *et al.* first reported an ambipolar BP transistor using a Al_2O_3 capping layer,[45] which is mainly attributed to the reduction of the effective Schottky barrier heights for electrons due to the fixed charges in the Al_2O_3 capping layer. The similar change from p-type to ambipolar is also reported by Haratipour *et al.* using locally back-gated BP transistors with 10 nm HfO_2 gate dielectric and Al_2O_3 capping layer.[46] The n-channel g_m is as high as 80 μS/μm. Li *et al.* measured an ambipolar BP transistor with a channel length of 0.2 μm and the maximum drain current is up to 85 μA/μm at room temperature.[47] Very recently, high-performance n-

type BP transistors have been reported using Al as the contact material.[48] The electron mobility can reach 275 and 630 $cm^2/(V\cdot s)$ at 300 and 80 K, respectively. Much work has also experimentally demonstrated n-type carrier transport in BP using doping by cross-linked PMMA,[49] Cs_2CO_3,[50] Cu atoms,[51] or Al atoms.[52] The transport polarity of the BP channel is closely related with the its channel thickness, contact metal, channel length, and doping. First, thicker body has small bandgap, leading to small Schottky barriers for both n- and p-transport, enabling ambipolar operation.[48,53] Second, low work function metal favors electron transport and high work function metal is beneficial to hole transport due to band alignment.[48] Third, for short channel devices, drain voltage also has an important effect on Schottky barriers in source/drain and changes the carrier transport.[54] Finally, the existence of mobile or fixed charges could introduce doping.[45]

Novel electronic device structures have also been demonstrated based on BP materials. Recently, Liu *et al.* reported a theoretical investigation of ballistic transport in multilayer BP tunneling FETs (TFETs) which can reach larger on-state current at the same I_{on}/I_{off} ratio compared to TMDs-based TFETs.[55] Constantinescu *et al*. found that the bandgap of the BP/hBN/BP heterostructure is highly tunable under electric field and the device exhibits negative differential resistance behavior.[56] Kang *et al*. fabricated a vertical field-effect transistor based on a graphene/BP van der Waals heterostructure.[57] The on-state current density is over 1600 A/cm^2 and current on/off ratio exceeds 800 at low temperatures.

3.2. Contact resistance

High contact resistance value limits the flow of current between the metal contacts and BP, which is critical for the realization of the ultra-scaled low-power transistors and the photonic devices such as solar cells and phototransistors.[58,59] It is well known that in conventional Si FETs a substitutional doping scheme is used to minimize the contact resistance. However, doping the atomically thin 2D materials is challenging and there is no available sustainable doping scheme.[60] Since metal-2D contacts are characterized by Schottky barriers (SBs), one has to minimize the height and width of the SB to improve the current.[61] One straightforward approach is to use metals with different work functions to minimize contact resistance and improve current.[62,63] Du *et al*. observed that Pd was better than Ni in order to reach higher output current of BP FETs.[54] The Pd contact resistance is 1.75 $k\Omega\cdot\mu m$ at $V_{bg} = -40$ V, which is smaller than the Ni contact resistance of 3.15 $k\Omega\cdot\mu m$ at the same back gate voltage. This is because that the work function of Pd is 5.4 eV which is higher than 5.0 eV of Ni, resulting in a smaller SB value. Very recently, a chemical doping method was developed to reduce the Ni contact resistance to 1.3 $k\Omega\cdot\mu m$ at $V_{bg} = -40$ V.[42] Meanwhile, the increase of electrostatically doped carrier density in BP under the metal contacts can also lead to a narrower Schottky barrier and reduce contact resistance. This was demonstrated by Haratipour *et al*., using a locally back-gated BP FET with 7-nm-thick HfO_2 gate dielectrics. The contact resistance value is as low as 1.14 $k\Omega\cdot\mu m$ using the Ti contact.[40] Although it is reported that graphene is a good contact material for TMDs,[64] the studies on using graphene for BP are still lacking.[65] Padilha *et al*. used *ab initio* simulations to study the contact properties of phosphorene and graphene and predicted that it was possible to achieve an ohmic contact for the bilayer system.[66]

To understand the switching mechanisms in few-layer BP transistors, Du *et al*. studied the effect of contact materials and channel length on transport behaviors of BP FETs.[54] It is observed that ambipolar behavior becomes much more pronounced if low-work-function-metal Ni is used for BP FETs at shorter channel lengths. This indicated that the Ni metal Fermi level is closer to the conduction band with minimal Fermi level pinning at the metal/BP interface. Due to the small band gap of BP, the transport types are closely correlated with the channel length, back gate voltages, and drain biases. For the long channel devices, the effective SB is only determined by gate bias. However, when reducing the channel length to sub-100 nm, the drain voltage can also modulate the effective SBs. An increase of the drain bias causes the decrease of the source barrier, leading to the injection of electrons into the conduction band, and the devices would exhibit stronger ambipolar behavior with enhanced n-type currents.

3.3. Radio frequency electronics

BP transistors are promising candidates for radio frequency (RF) applications because of the high mobility and velocity. The first RF transistor based on few-layer BP was demonstrated by Wang *et al*.,[67] with a short-circuit current-gain cutoff frequency f_T of 12 GHz and a maximum oscillation frequency f_{max} of 20 GHz from a 300 nm channel length device (Figs. 3(a) and 3(b)). Then Zhu *et al*. reported the first RF flexible BP thin-film transistors on highly bendable polyimide substrate.[68] The measured results showed an intrinsic maximum oscillation frequency f_{max} of 14.5 GHz and cutoff frequency f_T of 17.5 GHz at a channel length of 0.5 μm (Figs. 3(c) and 3(d)). The extracted saturation velocity of $\sim 6\times 10^6$ cm/s is more than an order of magnitude higher than the effective velocities achieved for MoS_2, IGZO, and poly-Si. Meanwhile, Chowdhury *et al*. investigated various BP-based RF circuits such as amplifier, mixer and AM demodulator with megahertz operating frequencies.[69] These results clearly reveal the great potential of BP transistors for power and voltage amplifiers in high-frequency electronics.

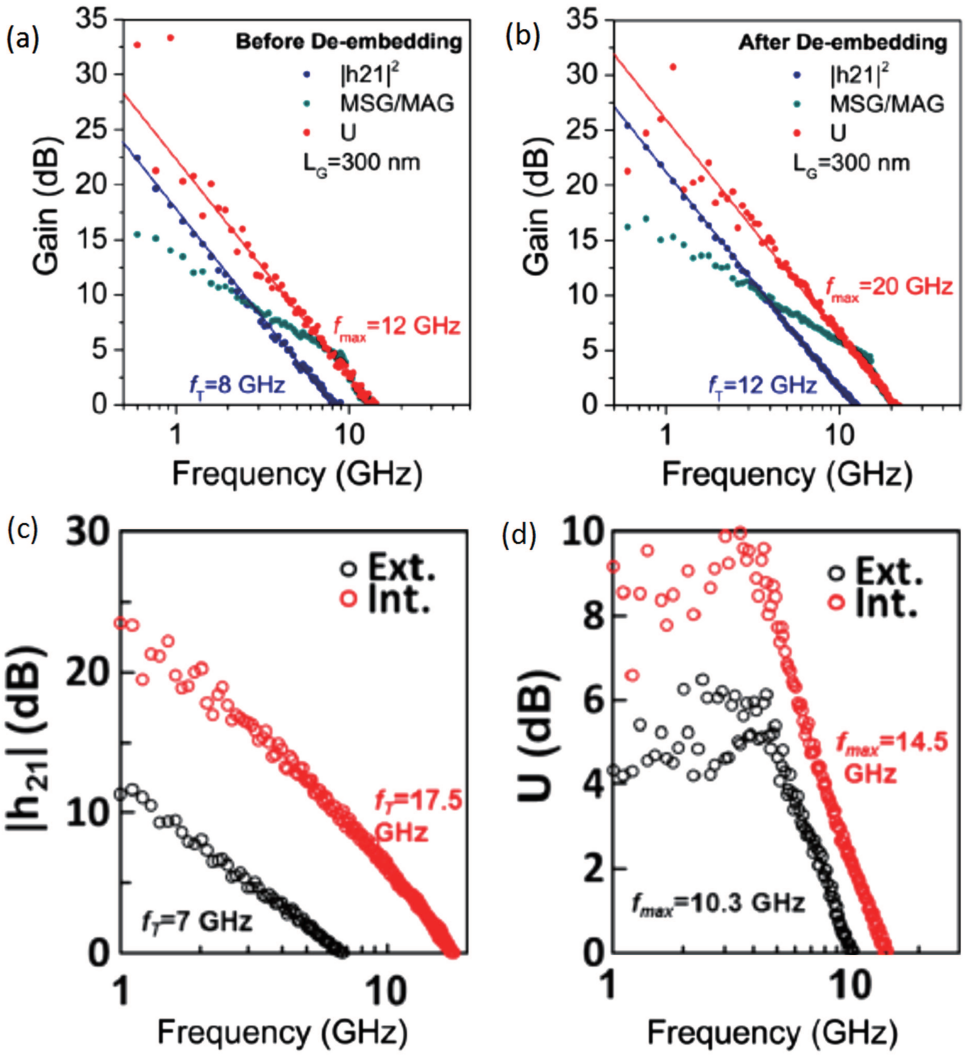


Fig. 3. (color online) Radio-frequency performance of the BP RF transistor. The short-circuit current gain h_{21}, MSG/MAG, and unilateral power gain U of the 300 nm channel length device (a) before and (b) after de-embedding.[67] (c) Short-circuit current gain $|h_{21}|$ before (extrinsic) and after (intrinsic) standard de-embedding of the 500 nm channel length device.[68] (d) Unilateral power gain, U, featuring extrinsic and intrinsic $f_{MAX} \sim 10.3$ and 14.5 GHz of the 500 nm channel length device.[68]

3.4. Short channel and quantum transport

The smallest channel length of the BP transistors is reported by Miao *et al.* with a channel length of 20 nm, which has an on-state current of 174 μA/μm at V_d of 0.1 V.[70] To fully explore the advantages of few-layer BP, reducing the contact resistance is of great importance to improve performance (particularly for short-channel devices). Only a few studies on metal-BP contacts have been published and more work is needed to understand the contact properties both theoretically and experimentally.[62,63] Hexagonal boron nitride (h-BN) is an ideal substrate to achieve high mobility of BP, which has been demonstrated to preserve the ultra-high mobility of graphene previously.[71,72] The schematic of the device is shown in Fig. 4(a). Due to the fact that the surface of the h-BN substrate is ultraflat and free of dangling bonds with greatly reduced scattering centers for BP, BP/BN heterostructure allows for a record-high field-effect mobility for both holes (3900 $cm^2/(V{\cdot}s)$) and electrons (1600 $cm^2/(V{\cdot}s)$) at $T =$ 1.5 K.[73] Pronounced Shubnikov–de Haas (SdH) oscillations are observed with both hole doping ($V_g < 0$) and electron doping ($V_g > 0$). The filling factors ν at each valley indicated that the transport is already in the extreme quantum limit as shown in Fig. 4(b). Chen *et al.* fabricated a BN/BP/BN heterostructure with a high field-effect mobility of 1350 $cm^2/(V{\cdot}s)$ at room temperature as shown in Figs. 4(c) and 4(d).[74] Quantum oscillations in BP two-dimensional hole gas are also observed at low magnetic fields. Figure 4(e) shows the temperature dependence of resistivity ΔR, producing a cyclotron effective mass $0.27 \pm 0.02 m_e$ at $V_g = -60$ V. Gillgren *et al.* also demonstrated that h-BN/phosphorene/h-BN heterostructures with 1D edge contacts enable exploration of gate-tunable SdH magneto-oscillations and Zeeman splitting.[75] After that, the SdH oscillations were also observed in a 47 ± 1 nm two-terminal BP FET on SiO_2 substrates.[76] Kim *et al.* realized a widely tunable band gap and anisotropic Dirac semimetal state in few-layer BP by means of depositing potassium (K) atoms *in situ*.[77] This result provided great flexibility in design and optimization of BP-based electronic and optoelectronic devices.

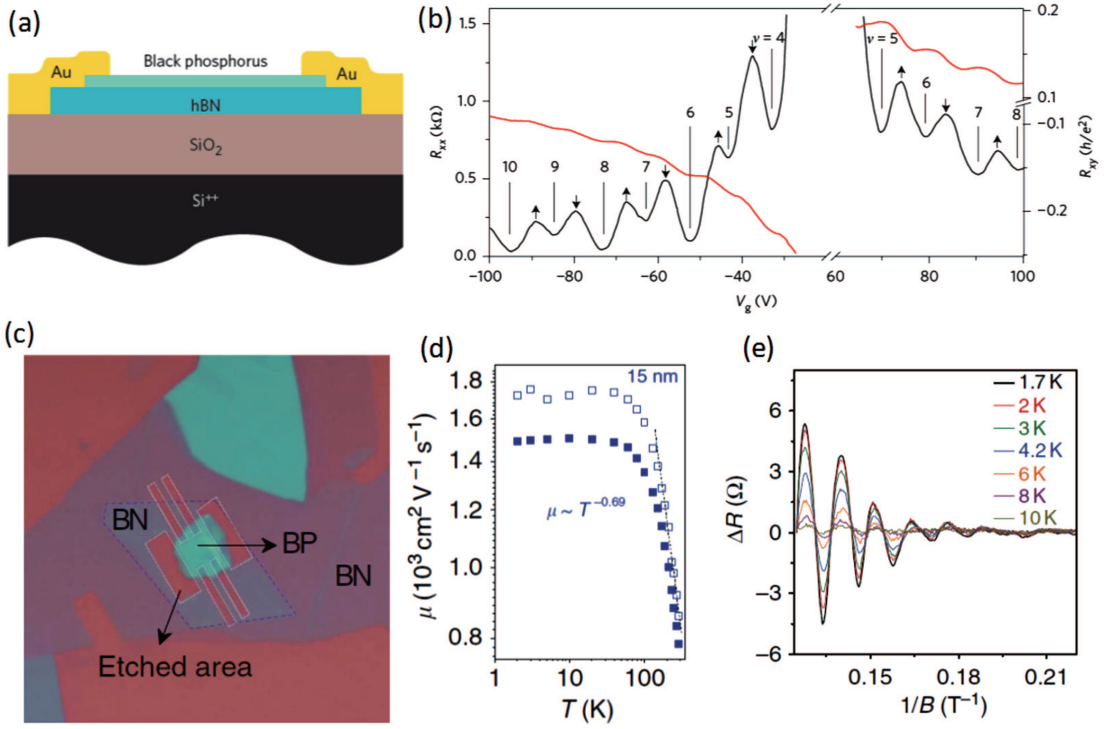


Fig. 4. (color online) (a) Schematic cross-sectional view of the BP FET structure with a h-BN substrate.[73] (b) R_{xx} (black) and R_{xy} (red) measured as a function of V_g with magnetic field fixed at $B = 31$ T and $T = 0.3$ K. Spin degeneracy is lifted at each LL, and the arrows indicate the spin-up and spin-down LLs.[73] (c) Schematic of the BN–BP–BN heterostructure device, the purple-dashed line denotes the lower BN layer.[74] (d) Temperature dependence of the field-effect μ_F (open dots) and Hall mobility μ_h (solid dots) at $V_g = -70$ V of 15-nm-thick sample. The dashed lines serve as guidelines for the $\mu \sim T^{-\gamma}$ relation.[74] (e) ΔR plotted as a function of $1/B$ at $V_g = -60$ V for different temperatures.

3.5. Stability

Few-layer BP materials exhibit high reactivity with water and oxygen, resulting in compositional and physical changes of the material with consequent degradation of its electronic properties. This poses a severe challenge for practical device applications in semiconductor technology and flexible electronics. Figure 5(a) compares the electrical properties of few-layer BP FETs in vacuum and after exposure in air.[78] It is clear that the threshold voltage shifts toward more negative values and the drain current decreases dramaticlly. Figure 5(b) shows the evolution of transfer curves of BP transistors at different exposure times, indicating a strong p-type doping after absorbing water. Much work has been focused on understanding of the degradation process and a reliable method towards stable BP materials.[79–82] The degradation is mainly attributed to the formation of oxidized phosphorus species by reacting with O_2 and H_2O in air.[29] Wood *et al.* reported that AlO_x capping layer can effectively suppress the degradation of BP materials to maintain stable condition for over 2 weeks in ambient.[83] Kim *et al.* further improved the air stability by using double layer capping with dielectric and fluoropolymer films.[84] Favron *et al.* reported detailed transmission electron microscopy (TEM), electron-energy loss (TEM-EELS) and Raman spectroscopy characterizations that elucidate the rate of oxidation depends linearly on oxygen concentration and light intensity and exponentially on the square of the energy gap.[85] Figure 5(c) presents time dependence of the integrated intensity of the A_g^2 Raman mode in different conditions, showing that encapsulation with a 300 nm of parylene C can effectively protect BP. Other capping layer, such as poly(methyl methacrylate) (PMMA) and BN, have also been demonstrated recently.[76,86–88] Very recently, Ryder *et al.* proposed a covalent modification scheme to passivation BP and improves the electrical properties.[89] Ziletti *et al.* showed that oxygen chemisorption onto phosphorene caused the formation of neutral defects and metastable electrically active defects by using first-principles calculations.[90,91] Utt *et al.* theoretically studied the degradation dynamics of BP and found that intrinsic defects lower the chemisorption barrier of ideal BP, thus enabling the photoinduced oxidation of BP and the dissociation of oxygen dimers.[92] We believe that with more and more theoretical and experimental studies of the oxidation mechanisms, ultimate control or suppression of degradation can be realized to achieve stable BP devices.

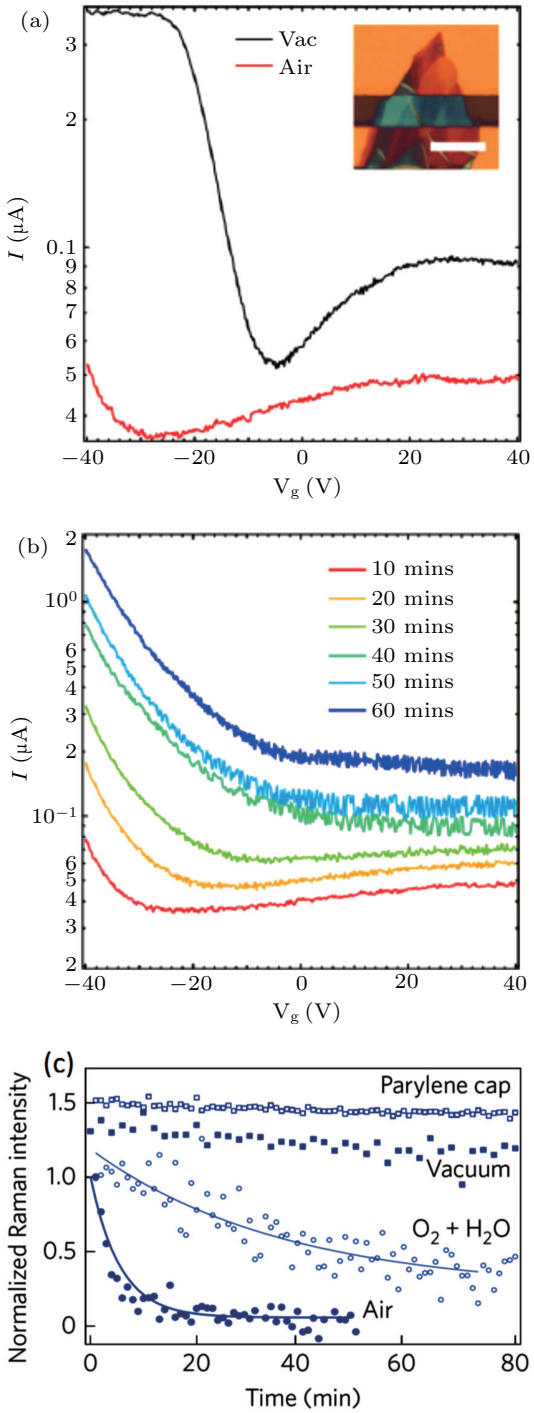


Fig. 5. (color online) (a) Transfer characteristics of the BP FET device in vacuum before exposure (black curve) and directly after breaking the vacuum (red curve) taken at $V_b = 100$ mV. Inset shows an optical image of a BP flake before longterm ambient exposure (scale bar is 10 μm).[78] (b) Transfer characteristics at selected times over the first hour of exposure.[78] (c) Time dependence of the integrated intensity of the A_g^2 Raman mode in different conditions: air, vacuum, mixture of O_2 and H_2O, and in air but encapsulated under a 300 nm layer of parylene cap.[85]

4. Optoelectronics properties

Extensive research on photodetectors based on novel 2D materials have been carried out recently because of their wide application in photodetection, imaging, and telecommunications.[93–95] Graphene photodetectors provide broadband detection from ultraviolet (UV) to Terahertz (THz), ultrafast response time, and tunable optical properties.[96,97] One issue is that its gapless nature causes low responsivity and low photoconductive gain which could limit its application.[93] Compared with graphene-based photodetectors, TMDs possess sizable energy gap which leads to lower dark currents and higher responsivity as long as they are direct bandgap, but the operation speed and response spectrum range are limited.[18,98] The direct bandgap from monolayer to bulk (2.0 eV to $\sim$ 0.3 eV) of BP covers a regime otherwise unavailable from other 2D layered materials.[35] It bridges the band gap ranges between that of graphene (zero band gap) and TMDCs ($\sim$ 1.0 to 2.5 eV). Such a narrow bandgap covering the spectral range from visible to near-infrared makes BP a very promising candidate for broadband optoelectronic applications. For example, infrared photodetectors are highly desired for various demanding applications, e.g., telecommunication, thermal imaging, biological imaging, and remote sensing.[99,100] In addition to the high carrier mobility, the direct bandgap nature and strong light absorption efficiency in broadband spectrum makes BP ideal candidate for high performance photodetection. More importantly, BP exhibits in-plane anisotropy, which is not readily found in other 2D crystals derived from layered materials. This can be manifested in the optical, electrical, thermal, and mechanical properties of the resulting devices, and has potential for the realization of conceptually novel electronic, optoelectronic, and nano-mechanical devices.

4.1. Photodetectors

Photodetectors are devices used for the detection of light, which could convert light into electrical signals used in many applications, such as video imaging, optical communications, biomedical imaging, security, night-vision, gas sensing, and motion detection.[93] Here we discuss two different types of photodetector (photodiodes and photoconductors). A photodiode is a p–n junction or PIN structure which creates electron–hole pairs when photons of sufficient energy strike. This mechanism is also known as the inner photoelectric effect. If the absorption occurs in the junction's depletion region, or one diffusion length away from it, these carriers are swept from the junction by the built-in electric field of the depletion region. Thus holes and electrons move toward opposite directions and a photocurrent is produced.[94] When light is absorbed by a material such as a semiconductor, the number of free electrons and electron holes increases and raises its electrical conductivity and this is the photoconductive effect. There are several significant figure-of-merit parameters for evaluating the optical properties of photodetectors, including responsivity, internal and external quantum efficiencies, noise-equivalent power, detectivity and time response,

etc.[99,101,102] Responsivity (R) is the ratio of the photocurrent to the incident light power on the effective area. It is given by $R = I_{ph}/P_o$, where I_{ph} is the effective area and P_o is the incident light power. The external quantum efficiency (EQE) is the ratio of the number of the charge carriers in the photocurrent and the total number of incident photons. It can be written as: $EQE = (I_{ph}/q)/(P_o/hv) = R(hc)/(q\lambda)$, where q is electron charge, h Planck's constant, c is the speed of light, λ the wavelength of light, and v frequency of light. EQE can be increased by increasing the optical absorption of active layer and preventing the recombination or trapping of carriers before they are collected. Internal quantum efficiency (IQE) denotes the number of measured charge carriers divided by the number of absorbed photons. The IQE is always larger than the EQE. A low IQE indicates that the active layer of the device is unable to make good use of the photons to generate charge pairs. Noise-equivalent power (NEP) is the minimum illumination power that delivers a unity signal-to-noise ratio at 1 Hz bandwidth. It can be expressed as NEP = PSD/R where the PSD is the current noise power spectral density in dark (in A·Hz$^{-1/2}$) at 1 Hz bandwidth. Detectivity (D^*) can be expressed as $D^* = R/(2qJ_d)^{1/2}$, where R is the responsivity, q is the elementary charge, and J_d is the dark current density when the dark current is dominated by the shot noise. Time response is usually defined as the time necessary to increase the photoresponse from 10% to 90% on the rising edge or reduce the photoresponse from 90% to 10% on the falling edge. The photoconductive gain is the ratio of the photogenerated carrier lifetime (τ_{tr}) and the transit time ($\tau_{transit}$), which can be calculated by $G = \tau_{tr}/\tau_{transit}$. $\tau_{transit}$ is defined as $\tau_{transit} = L^2/(\mu V)$, where L is the channel length of the transistor, μ the charge carrier mobility, and V the source-drain bias.

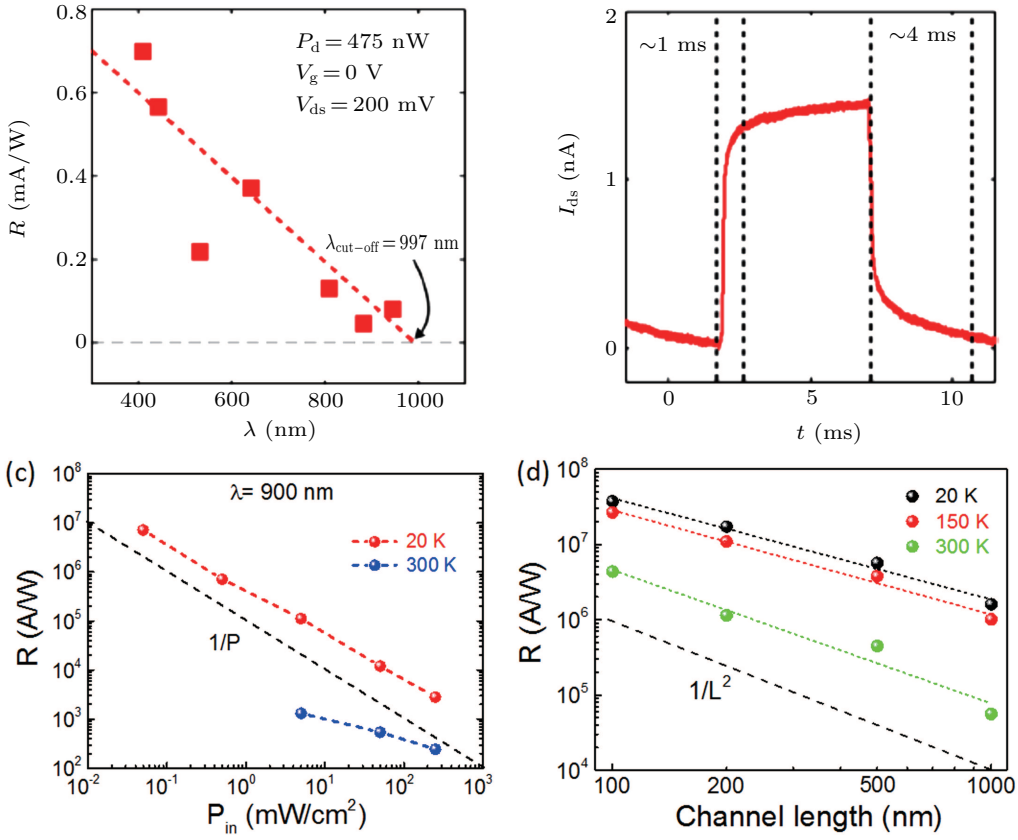


Fig. 6. (color online) (a) Responsivity versus excitation wavelength at constant power (red squares) of a BP photodetector. The dashed red line is a linear fit to the data.[103] (b) Photocurrent measured in one period of modulation of the light intensity ($\lambda = 640$ nm, $P_d = 6.49$ μW, $V_{ds} = 100$ mV). We can estimate a rise (fall) time of 1 ms (4 ms).[103] (c) R of the device at different incident laser power at 900 nm wavelength at room temperature and low temperature.[105] (d) Photoresponsivity of the different channel length devices under the same driving voltage.[105]

Buscema *et al.* made few-layer BP phototransistors for broadband and fast detection. The substrate is 285 nm SiO_2 and the contact materials are Ti/Au.[103] Owing to the high mobility and large on/off ratio of few-layer BP, the devices have a rise time of about 1 ms and can reach a photoresponsivity of 4.8 mA/W at wavelength of 640 nm, with an operational range from 400 nm to 997 nm (Figs. 6(a) and 6(b)). Deng *et al.* demonstrated a responsivity of 223 mA/W using a few-layer BP on 90 nm SiO_2. This improved responsivity is due to the fact that metals with larger work function (Pd) as contacts can significantly reduce the SB height for hole injection on a BP FET and improve the collection of photo-

induced carriers. Wu *et al.* revealed that the BP devices can also be configured as an excellent UV photodetector with a photoresponsivity of $\sim 10^5$ A/W.[104] However, the response speed is relatively slow and the photoresponsivity drops dramatically for almost five orders of magnitude as the excitation wavelength increases beyond 500 nm. One strategy to improve the photoresponsivity for this class of devices is to reduce the channel length, which has been demonstrated by Huang *et al*. The record-high photoresponsivity reaches up to about 7×10^6 A/W at 20 K and 4.3×10^6 A/W at 300 K for the 100 nm BP device in a broadband spectrum (Figs. 6(c) and 6(d)).[105] Viti *et al*. demonstrated BP terahertz photodetectors due to the excellent on–off ratios.[106] Very recently, Guo *et al*. showed BP mid-infrared detectors at 3.39 μm with high internal gain, resulting in an external responsivity of 82 A/W.[107] These findings indicate that 2D BP semiconductor are highly suitable for high-performance photodetectors in a variety of applications

4.2. Heterostructure

The p–n junctions are the building blocks of modern optoelectronic devices. One strategy to further improve the efficiency and photoresponsivity of these devices is to create heterojunctions based on BP and other 2D materials.[108,109] BP is a typical p-type semiconductor and MoS_2 is a n-type semiconductor. Deng *et al.* firstly demonstrated a gate-tunable van der Waals p–n diode by vertically stacking MoS_2 and BP (Fig. 7(a)).[110] These ultrathin p–n diodes show a maximum photodetection responsivity of 418 mA/W at the wavelength of 633 nm and photovoltaic energy conversion with an EQE of 0.3%. The responsivity reaches 1.27 A/W and 11 mA/W for forward and reverse bias, respectively (Fig. 7(b)). The improvement in responsibility is due to the fact that the built-in electric field in the heterojunction can allow for more efficient separation of the electron–hole pairs. However, the EQE of these devices is not good enough due to the relatively low carrier mobility in the lateral transport channels. Ye *et al*. reported a similar device structure with MoS_2 and BP for the near-infrared photodetector.[111] The photoresponsivity is 153.4 mA/W measured at $\lambda = 1.55$ μm with a response time of 15 μs. Chen *et al*. fabricated WSe_2-BP van der Waals heterojunction devices with improved EQE.[112] In addition, Buscema *et al*. used two local gates to control the local charge carrier type as well as density and realize a short-circuit current with illumination wavelengths up to 940 nm.[113] Recently, BP also demonstrates potential in high-speed data communication by integration on a silicon photonic waveguide operating in the near-infrared telecom band with a high response bandwidth exceeding 3 GHz.[114] Due to the finite bandgap, BP photodetectors can operate under bias with very low dark current and attain an intrinsic responsivity up to 135 mA/W at room temperature. The development of BP-based van der Waals heterostructures is at its early stage and more applications will be demonstrated in future

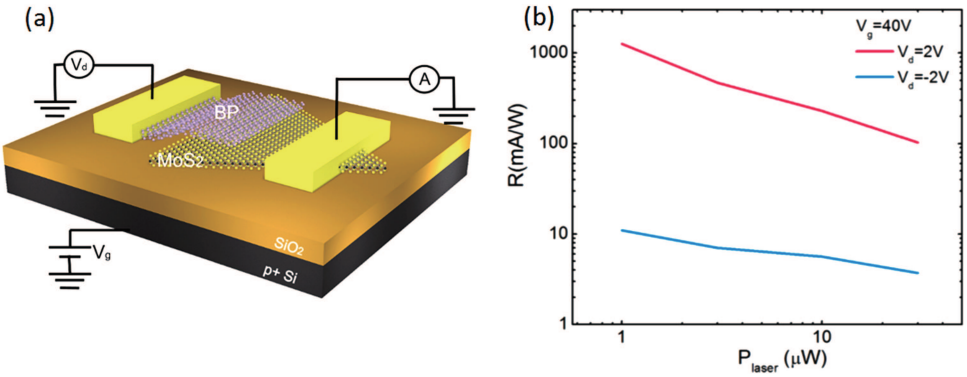


Fig. 7. (color online) (a) Schematics of the device structure. A heavily doped silicon wafer capped with 285 nm SiO_2 is used as the global back gate and the gate dielectric. Few-layer black phosphorus flakes were exfoliated onto monolayer MoS_2 in order to form a van der Waals heterojunction. (b) Photodetection R calculated as a function of incident power.[110]

4.3. Anisotropy

The most exciting advantage of BP is its in-plane anisotropy in the electronic,[6] optical,[38] phonon,[28] and mechanical properties compared to graphene and TMDs,[115] which provides opportunity and platform for new devices and applications.[116] Hong *et al*. reported spatially resolved polarization-dependent scanning photocurrent measurements on the BP FET.[117] The anisotropic feature of the photocurrent response near the BP-metal contact area primarily results from the direction-dependent absorption of the BP crystals. Recently, they also performed polarization-dependent photocurrent measurements of the BPMoS_2 p–n junction under laser illumination with different wavelengths.[118] If the incident photon energy is above the direct band gap of MoS_2 the photocurrent response at the p–n junction primarily depends on a competitive effect between BP and MoS_2. When the energy is below the direct band gap of MoS_2, the photocurrent response results from the direct band gap transition in BP. Wang *et al*. presented polarization-resolved photoluminescence spectra of some BP monolayer samples.[35] Ex-

citon photoluminescence with large in-plane anisotropy is attributed to the reduced symmetry and screening, which is consistent with previous theory studies.[119] Yuan *et al.* addressed a polarization-sensitive broadband photodetector using a black phosphorus vertical p–n junction with an electric-double-layer transistor configuration. These results show that BP might provide new design and functionalities in novel optical and electronic applications.

5. Conclusion and perspectives

In this review, we have summarized the recent progress in BP-based electronic and optoelectronic devices. Benefiting from the direct bandgap, high carrier mobility, and excellent anisotropy, BP devices exhibit superior performance in various applications. To better assess the potential of BP, we provide our perspectives for future investigation.

(i) Producing large area and high-quality BP material at low cost is essential for future applications.

(ii) Fabrication of silicon-compatible top-gated BP transistors with optimized interface is an important direction.

(iii) Improving the contact scheme and reducing the contact resistance are important for high-performance transistors.

(iv) High-field and ballistic transport for short channel devices need further investigations. The degradation mechanism and reliability need to be assessed.

(v) Develop high-performance BP radio frequency transistors and circuits.

(vi) Design novel van der Waals heterostructures with stacked 2D materials.

References

[1] Novoselov K S, Geim A K, Morozov S V, Jiang D, Zhang Y, Dubonos S V, Grigorieva I V and Firsov A A 2004 *Science* **306** 666

[2] Geim A K and Grigorieva I V 2013 *Nature* **499** 419

[3] Novoselov K, Jiang D, Schedin F, Booth T, Khotkevich V, Morozov S and Geim A 2015 *Proceedings of the National Academy of Sciences of the United States of America* **102** 10451

[4] Radisavljevic B, Radenovic A, Brivio J, Giacometti V and Kis A 2011 *Nat. Nanotechnol.* **6** 147

[5] Li L, Yu Y, Ye G J, Ge Q, Ou X, Wu H, Feng D, Chen X H and Zhang Y 2014 *Nat. Nanotechnol.* **9** 372

[6] Liu H, Neal A T, Zhu Z, Luo Z, Xu X, Tománek D and Ye P D 2014 *ACS Nano* **8** 4033

[7] Chhowalla M, Shin H S, Eda G, Li L J, Loh K P and Zhang H 2013 *Nat. Chem.* **5** 263

[8] Wang Q H, Kalantar-Zadeh K, Kis A, Coleman J N and Strano M S 2012 *Nat. Nanotechnol.* **7** 699

[9] Yoon Y, Ganapathi K and Salahuddin S 2011 *Nano Lett.* **11** 3768

[10] Fiori G, Bonaccorso F, Iannaccone G, Palacios T, Neumaier D, Seabaugh A, Banerjee S K and Colombo L 2014 *Nat. Nanotechnol.* **9** 768

[11] Schwierz F 2010 *Nat. Nanotechnol.* **5** 487

[12] Mak K F, Lee C, Hone J, Shan J and Heinz T F 2010 *Phys. Rev. Lett.* **105** 136805

[13] Liu H, Neal A T and Ye P D 2012 *ACS Nano* **6** 8563

[14] Zhu W, Low T, Lee Y H, Wang H, Farmer D B, Kong J, Xia F and Avouris P 2014 *Nat. Commun.* **5** 3087

[15] Li X, Yang L, Si M, Li S, Huang M, Ye P and Wu Y 2015 *Adv. Mater.* **27** 1547

[16] Wang H, Yu L, Lee Y H, Shi Y, Hsu A, Chin M L, Li L J, Dubey M, Kong J and Palacios T 2012 *Nano Lett.* **12** 4674

[17] Cheng R, Jiang S, Chen Y, Liu Y, Weiss N, Cheng H C, Wu H, Huang Y and Duan X 2014 *Nat. Commun.* **5** 5143

[18] Lopez-Sanchez O, Lembke D, Kayci M, Radenovic A and Kis A 2013 *Nat. Nanotechnol.* **8** 497

[19] Xia F, Wang H, Xiao D, Dubey M and Ramasubramaniam A 2014 *Nat. Photon.* **8** 899

[20] Kaasbjerg K, Thygesen K S and Jacobsen K W 2012 *Phys. Rev. B* **85** 115317

[21] Jariwala D, Sangwan V K, Lauhon L J, Marks T J and Hersam M C 2014 *ACS Nano* **8** 1102

[22] Du Y, Yang L, Liu H and Peide D Y 2014 *APL Mater.* **2** 092510

[23] Morita A 1986 *Appl. Phys. A* **39** 227

[24] Xia F, Wang H and Jia Y 2014 *Nat. Commun.* **5** 4458

[25] Ling X, Wang H, Huang S, Xia F and Dresselhaus M S 2015 *Proceedings of the National Academy of Sciences* **112** 4523

[26] Wang X, Jones A M, Seyler K L, Tran V, Jia Y, Zhao H, Wang H, Yang L, Xu X and Xia F 2015 *Nat. Nanotechnol.* **10** 517

[27] Tran V, Soklaski R, Liang Y and Yang L 2014 *Phys. Rev. B* **89** 235319

[28] Qiao J, Kong X, Hu Z X, Yang F and Ji W 2014 *Nat. Commun.* **5** 4475

[29] Yau S L, Moffat T P, Bard A J, Zhang Z and Lerner M M 1992 *Chem. Phys. Lett.* **198** 383

[30] He J, He D, Wang Y, Cui Q, Bellus M Z, Chiu H Y and Zhao H 2015 *ACS Nano* **9** 6436

[31] Mao N, Tang J, Xie L, Wu J, Han B, Lin J, Deng S, Ji W, Xu H and Liu K 2015 *J. Am. Chem. Soc.* **138** 300

[32] Fei R and Yang L 2014 *Nano Lett.* **14** 2884

[33] Carvalho A, Wang M, Zhu X, Rodin A S, Su H and Castro Neto A H 2016 *Nat. Rev. Mater.* **1** 16061

[34] Yang J, Xu R, Pei J, Myint Y W, Wang F, Wang Z, Zhang S, Yu Z and Lu Y 2015 *Light: Science & Applications* **4** e312

[35] Wang X, Jones A M, Seyler K L, Tran V, Jia Y, Zhao H, Wang H, Yang L, Xu X and Xia F 2015 *Nat. Nanotechnol.* **10** 517

[36] Liu Y, Low T and Ruden P P 2016 *Phys. Rev. B* **93** 165402

[37] Liu H, Du Y, Deng Y and Ye P D 2015 *Chem. Soc. Rev.* **44** 2732

[38] Xia F, Wang H and Jia Y 2014 *Nat. Commun.* **5** 4485

[39] Cao X and Guo J 2015 *IEEE Trans. Electron Devices* **62** 659

[40] Haratipour N, Robbins M C and Koester S J 2015 *IEEE Electron Dev. Lett.* **36** 411

[41] Haratipour N, Namgung S, Oh S H and Koester S J 2016 *ACS Nano* **10** 3791

[42] Du Y, Yang L, Zhou H and Ye P D 2016 *IEEE Electron Dev. Lett.* **37** 429

[43] Li L, Engel M, Farmer D B, Han S j and Wong H S P 2016 *ACS Nano* **10** 4672

[44] Zhu W, Yogeesh M N, Yang S, Aldave S H, Kim J S, Sonde S, Tao L, Lu N and Akinwande D 2015 *Nano Lett.* **15** 1883

[45] Liu H, Neal A T, Si M, Du Y and Ye P D 2014 *IEEE Electron Dev. Lett.* **35** 795

[46] Haratipour N and Koester S J 2016 *IEEE Electron Dev. Lett.* **37** 103

[47] Li X, Du Y, Si M, Yang L, Li S, Li T, Xiong X, Ye P and Wu Y 2016 *Nanoscale* **8** 3572

[48] Perello D J, Chae S H, Song S and Lee Y H 2015 *Nat. Commun.* **6** 7809

[49] Wang G, Bao L, Pei T, Ma R, Zhang Y Y, Sun L, Zhang G, Yang H, Li J, Gu C, Du S, Pantelides S T, Schrimpf R D and Gao H J 2016 *Nano Lett.* **16** 6870

[50] Xiang D, Han C, Wu J, Zhong S, Liu Y, Lin J, Zhang X A, Ping H W, Özyilmaz B, Neto A H C, Wee A T S and Chen W 2015 *Nat. Commun.* **6** 6485

[51] Koenig S P, Doganov R A, Seixas L, Carvalho A, Tan J Y, Watanabe K, Taniguchi T, Yakovlev N, Castro Neto A H and Özyilmaz B 2016 *Nano Lett.* **16** 2145

[52] Prakash A, Cai Y, Zhang G, Zhang Y W and Ang K W 2017 *Small* **13** 1602909

[53] Penumatcha A V, Salazar R B and Appenzeller J 2015 *Nat. Commun.* **6** 8948

[54] Du Y, Liu H, Deng Y and Ye P D 2014 *ACS Nano* **8** 10035

[55] Liu F, Shi Q, Wang J and Guo H 2015 *Appl. Phys. Lett.* **107** 203501

[56] Constantinescu G C and Hine N D 2016 *Nano Lett.* **16** 2586

[57] Kang J, Jariwala D, Ryder C R, Wells S A, Choi Y, Hwang E, Cho J H, Marks T J and Hersam M C 2016 *Nano Lett.* **16** 2580

[58] Penumatcha A V, Salazar R B and Appenzeller J 2015 *Nat. Commun.* **6** 8948
[59] Du Y, Neal A T, Zhou H and Ye P D 2016 *J. Phys.: Condens. Mat.* **28** 263002
[60] Allain A, Kang J, Banerjee K and Kis A 2015 *Nat. Mater.* **14** 1195
[61] Pan Y, Wang Y, Ye M, Quhe R, Zhong H, Song Z, Peng X, Yu D, Yang J, Shi J and Lu J 2016 *Chem. Mater.* **28** 2100
[62] Chanana A and Mahapatra S 2014 *J. Appl. Phys.* **116** 204302
[63] Gong K, Zhang L, Ji W and Guo H 2014 *Phys. Rev. B* **90** 125441
[64] Cui X, Lee G H, Kim Y D, Arefe G, Huang P Y, Lee C H, Chenet D A, Zhang X, Wang L and Ye F 2015 *Nat. Nanotechnol.* **10** 534
[65] Avsar A, Vera-Marun I J, Tan J Y, Watanabe K, Taniguchi T, Castro Neto A H and Ozyilmaz B 2015 *ACS Nano* **9** 4138
[66] Padilha J, Fazzio A and da Silva A J 2015 *Phys. Rev. Lett.* **114** 066803
[67] Wang H, Wang X, Xia F, Wang L, Jiang H, Xia Q, Chin M L, Dubey M and Han S J 2014 *Nano Lett.* **14** 6424
[68] Zhu W, Park S, Yogeesh M N, McNicholas K M, Bank S R and Akinwande D 2016 *Nano Lett.* **16** 2301
[69] Chowdhury S F, Yogeesh M N, Banerjee S K and Akinwande D 2016 *IEEE Electron Dev. Lett.* **37** 449
[70] Miao J, Zhang S, Cai L, Scherr M and Wang C 2015 *ACS Nano* **9** 9236
[71] Dean C R, Young A F, Meric I, Lee C, Wang L, Sorgenfrei S, Watanabe K, Taniguchi T, Kim P and Shepard K 2010 *Nat. Nanotechnol.* **5** 722
[72] Li X, Lu X, Li T, Yang W, Fang J, Zhang G and Wu Y 2015 *ACS Nano* **9** 11382
[73] Li L, Ye G J, Tran V, Fei R, Chen G, Wang H, Wang J, Watanabe K, Taniguchi T and Yang L 2015 *Nat. Nanotechnol.* **10** 608
[74] Chen X, Wu Y, Wu Z, Han Y, Xu S, Wang L, Ye W, Han T, He Y and Cai Y 2015 *Nat. Commun.* **6** 7315
[75] Chen P, Xiang J, Yu H, Xie G, Wu S, Lu X, Wang G, Zhao J, Wen F and Liu Z 2015 *2D Materials* **2** 034009
[76] Tayari V, Hemsworth N, Fakih I, Favron A, Gaufres E, Gervais G, Martel R and Szkopek T 2015 *Nat. Commun.* **6** 7702
[77] Kim J, Baik S S, Ryu S H, Sohn Y, Park S, Park B G, Denlinger J, Yi Y, Choi H J and Kim K S 2015 *Science* **349** 723
[78] Island J O, Steele G A, van der Zant H S and Castellanos-Gomez A 2015 *2D Materials* **2** 011002
[79] Boukhvalov D W, Rudenko A N, Prishchenko D A, Mazurenko V G and Katsnelson M I 2015 *PCCP* **17** 15209
[80] Luo X, Rahbarihagh Y, Hwang J C M, Liu H, Du Y and Ye P D 2014 *IEEE Electron Dev. Lett.* **35** 1314
[81] Castellanos-Gomez A, Vicarelli L, Prada E, Island J O, Narasimha-Acharya K, Blanter S I, Groenendijk D J, Buscema M, Steele G A and Alvarez J 2014 *2D Materials* **1** 025001
[82] Gao J, Zhang G and Zhang Y W 2016 *J. Am. Chem. Soc.* **138** 4763
[83] Wood J D, Wells S A, Jariwala D, Chen K S, Cho E, Sangwan V K, Liu X, Lauhon L J, Marks T J and Hersam M C 2014 *Nano Lett.* **14** 6964
[84] Kim J S, Liu Y, Zhu W, Kim S, Wu D, Tao L, Dodabalapur A, Lai K and Akinwande D 2015 *Sci. Rep.* **5** 8989
[85] Favron A, Gaufrès E, Fossard F, Phaneuf-L'Heureux A L, Tang N Y, Lévesque P L, Loiseau A, Leonelli R, Francoeur S and Martel R 2015 *Nat. Mater.* **14** 826
[86] Avsar A, Vera-Marun I J, Tan J Y, Watanabe K, Taniguchi T, Castro Neto A H and Özyilmaz B 2015 *ACS Nano* **9** 4138
[87] Engel M, Steiner M and Avouris P 2014 *Nano Lett.* **14** 6414
[88] Doganov R A, O'Farrell E C T, Koenig S P, Yeo Y, Ziletti A, Carvalho A, Campbell D K, Coker D F, Watanabe K, Taniguchi T, Neto A H C and Ozyilmaz B 2015 *Nat. Commun.* **6** 6647
[89] Ryder C R, Wood J D, Wells S A, Yang Y, Jariwala D, Marks T J, Schatz G C and Hersam M C 2016 *Nat. Chem.* **8** 597
[90] Ziletti A, Carvalho A, Campbell D K, Coker D F and Castro Neto A H 2015 *Phys. Rev. Lett.* **114** 046801
[91] Wang V, Kawazoe Y and Geng W 2015 *Phys. Rev. B* **91** 045433
[92] Utt K L, Rivero P, Mehboudi M, Harriss E O, Borunda M F, Pacheco SanJuan A A and Barraza-Lopez S 2015 *ACS Central Science* **1** 320
[93] Koppens F H L, Mueller T, Avouris P, Ferrari A C, Vitiello M S and Polini M 2014 *Nat. Nanotechol.* **9** 780
[94] Xia F, Wang H, Xiao D, Dubey M and Ramasubramaniam A 2014 *Nat. Photon.* **8** 899
[95] Mak K F and Shan J 2016 *Nat. Photon.* **10** 216
[96] Xia F, Mueller T, Lin Y m, Valdes-Garcia A and Avouris P 2009 *Nat. Nanotechnol.* **4** 839
[97] Tielrooij K J, Piatkowski L, Massicotte M, Woessner A, Ma Q, Lee Y, Myhro K S, Lau C N, Jarillo Herrero P, van Hulst N F and Koppens F H L 2015 *Nat. Nanotechnol.* **10** 437
[98] Yin Z, Li H, Li H, Jiang L, Shi Y, Sun Y, Lu G, Zhang Q, Chen X and Zhang H 2012 *ACS Nano* **6** 74
[99] Konstantatos G and Sargent E H 2010 *Nat. Nanotechnol.* **5** 391
[100] Rogalski A, Antoszewski J and Faraone L 2009 *J. Appl. Phys.* **105** 091101
[101] Buscema M, Island J O, Groenendijk D J, Blanter S I, Steele G A, van der Zant H S J and Castellanos-Gomez A 2015 *Chem. Soc. Rev.* **44** 3691
[102] Li J, Niu L, Zheng Z and Yan F 2014 *Adv. Mater.* **26** 5239
[103] Buscema M, Groenendijk D J, Blanter S I, Steele G A, van der Zant H S and Castellanos-Gomez A 2014 *Nano Lett.* **14** 3347
[104] Wu J, Koon G K W, Xiang D, Han C, Toh C T, Kulkarni E S, Verzhbitskiy I, Carvalho A, Rodin A S, Koenig S P, Eda G, Chen W, Neto A H C and Özyilmaz B 2015 *ACS Nano* **9** 8070
[105] Huang M, Wang M, Chen C, Ma Z, Li X, Han J and Wu Y 2016 *Adv. Mater.* **28** 3481
[106] Viti L, Hu J, Coquillat D, Knap W, Tredicucci A, Politano A, Vitiello M S 2015 *Adv. Mater.* **27** 5567
[107] Guo Q, Pospischil A, Bhuiyan M, Jiang H, Tian H, Farmer D, Deng B, Li C, Han S J, Wang H, Xia Q, Ma T P, Mueller T and Xia F 2016 *Nano Lett.* **16** 4648
[108] Wenjing Z, Qixing W, Yu C, Zhuo W and Andrew T S W 2016 *2D Materials* **3** 022001
[109] Tian H, Chin M L, Najmaei S, Guo Q, Xia F, Wang H and Dubey M 2016 *Nano Research* **9** 1543
[110] Deng Y, Luo Z, Conrad N J, Liu H, Gong Y, Najmaei S, Ajayan P M, Lou J, Xu X and Ye P D 2014 *ACS Nano* **8** 8292
[111] Ye L, Li H, Chen Z and Xu J 2016 *ACS Photonics* **3** 692
[112] Chen P, Zhang T T, Zhang J, Xiang J, Yu H, Wu S, Lu X, Wang G, Wen F, Liu Z, Yang R, Shi D and Zhang G 2016 *Nanoscale* **8** 3254
[113] Buscema M, Groenendijk D J, Steele G A, van der Zant H S J and Castellanos-Gomez A 2014 *Nat. Commun.* **5** 4651
[114] Youngblood N, Chen C, Koester S J and Li M 2015 *Nat. Photon.* **9** 247
[115] Wang Z, Jia H, Zheng X Q, Yang R, Ye G, Chen X and Feng P X L 2016 *Nano Lett.* **16** 5394
[116] Cai Y, Ke Q, Zhang G, Feng Y P, Shenoy V B and Zhang Y W 2015 *Adv. Funct. Mater.* **25** 2230
[117] Hong T, Chamlagain B, Lin W, Chuang H J, Pan M, Zhou Z and Xu Y Q 2014 *Nanoscale* **6** 8978
[118] Hong T, Chamlagain B, Wang T, Chuang H J, Zhou Z and Xu Y Q 2015 *Nanoscale* **7** 18537
[119] Li P and Appelbaum I 2014 *Phys. Rev. B* **90** 115439